Geophysical Research Letters

RESEARCH LETTER
10.1029/2018GL079067

Two-Dimensional Particle-in-Cell Simulation of Magnetosonic Wave Excitation in a Dipole Magnetic Field

Lunjin Chen[1], Jicheng Sun[1,2], Quanming Lu[2], Xueyi Wang[3], Xinliang Gao[2], Dedong Wang[4], and Shui Wang[2]

[1]W. B. Hanson Center for Space Sciences, Department of Physics, University of Texas at Dallas, Richardson, TX, USA, [2]CAS Key Laboratory of Geospace Environment, Department of Geophysics and Planetary Science, University of Science and Technology of China, Hefei, China, [3]Physics Department, Auburn University, Auburn, AL, USA, [4]GFZ German Research Center for Geosciences, Potsdam, Germany

Key Points:
- Two-dimensional particle-in-cell simulation of magentosonic wave excitation in a dipole magnetic field is presented for the first time
- The waves are excited in the localized source region with bidirectional (inward and outward) propagation and propagates outside
- Excited magnetosonic waves lead to perpendicular heating of the cool protons and parallel heating of cool electrons

Correspondence to:
Q. Lu,
qmlu@ustc.edu.cn

Citation:
Chen, L., Sun, J., Lu, Q., Wang, X., Gao, X., Wang, D., & Wang, S. (2018). Two-dimensional particle-in-cell simulation of magnetosonic wave excitation in a dipole magnetic field. *Geophysical Research Letters*, *45*, 8712–8720. https://doi.org/10.1029/2018GL079067

Received 3 JUN 2018
Accepted 30 JUL 2018
Accepted article online 6 AUG 2018
Published online 5 SEP 2018

Abstract The excitation of magnetosonic waves in the meridian plane of a rescaled dipole magnetic field is investigated, for the first time, using a general curvilinear particle-in-cell simulation. Our simulation demonstrates that the magnetosonic waves are excited near the equatorial plane by tenuous ring distribution protons. The waves propagate nearly perpendicularly to the background magnetic field along both radially inward and outward directions. Different speeds of inward and outward propagation result in the asymmetrical distribution about the source region. The waves are accompanied by energization of both cool protons and electrons near the wave source region. The cool protons are heated perpendicularly, while the cool electrons can be heated in the parallel direction and also experience enhanced perpendicular drift at the presence of intense wave power. The implications of simulation results to the observations of magnetosonic waves and related particle heating in the inner magnetosphere are also discussed.

Plain Language Summary The Earth's radiation belt is a natural space environment consisting of relativistic electrons trapped in geospace. It exhibits great variability due to solar activities and poses a great threat to spacecraft orbiting in the regions and to astronauts. The primary physical process involved for radiation belt variability is through interaction with electromagnetic waves. Magnetosonic waves are one of the important waves that are capable of electron scattering, the efficiency of which depends on the wave detailed properties. Previous simulation has investigated the wave excitation in a homogeneous plasma. Here we present for the first time a 2-D particle-in-cell simulation to understand magnetosonic wave excitation and propagation in an inhomogeneous dipole magnetic field. The simulation results not only illustrate the wave temporal evolution and spatial distribution, both in radial and latitudinal distribution, but also reveal their effects on thermal electron and proton heating. These results are ready for verification against wave and particle measurement from the ongoing magnetospheric missions such as Van Allen Probes.

1. Introduction

Equatorial magnetosonic waves are usually observed around the Earth's magnetic equator within $2 < L < 8$ (Boardsen et al., 2014; Gurnett, 1976; Russell et al., 1970; Santolík et al., 2002; Tsurutani et al., 2014). These electromagnetic emissions, which propagate nearly perpendicularly to the background magnetic field, typically exhibit a series of harmonics of the proton gyrofrequency up to the lower hybrid frequency (e.g., Balikhin et al., 2015). The waves are receiving more and more attention because of their potential roles in both accelerating and scattering relativistic electrons in the radiation belt through Landau resonance (Horne et al., 2007; Li et al., 2014, 2016), transit time effects (Bortnik & Thorne, 2010; Bortnik et al., 2015), and bounce resonance (Chen et al., 2015; Li et al., 2015; Tao & Li, 2016). Magnetosonic waves in the inner magnetosphere are also known as equatorial noises and ion Bernstein modes, and we refer to them as magnetosonic waves hereafter.

Satellite observations (Boardsen et al., 1992; Ma et al., 2014; Meredith et al., 2008; Min et al., 2018; Perraut et al., 1982) have shown a close relation between the excitation of magnetosonic waves and a ring-like (or partial shell) distribution of tenuous energetic protons, and theoretical calculations (Chen, 2015; Chen, Thorne, Jordanova, & Horne, 2010; Curtis & Wu, 1979; Gul'elmi et al., 1975; McClements et al., 1994; Min & Liu, 2016; Sun, Gao, Chen, et al., 2016; Yuan et al., 2017) have verified that a proton ring distribution with the ring velocity

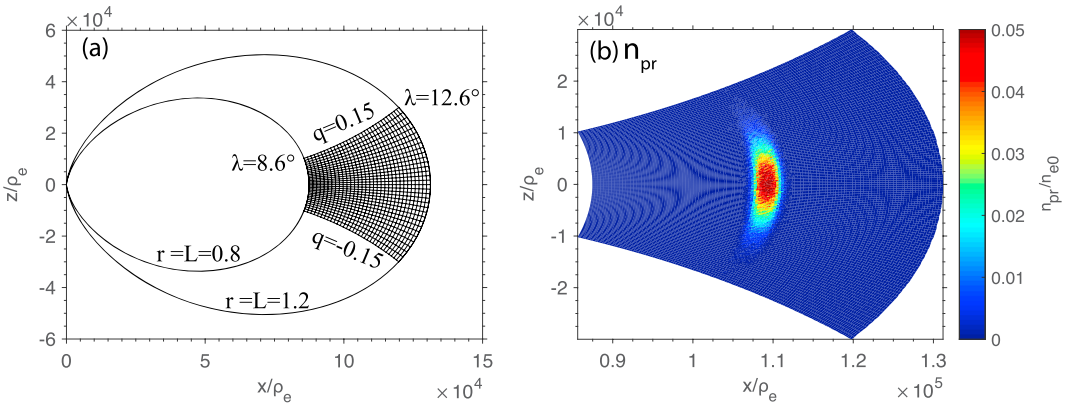

Figure 1. (a) The simulation domain shaded in black in Cartesian (x, z) coordinates on the meridian plane normalized by electron gyroradius ρ_e. The black lines represent the magnetic field lines. (b) The initial number density of ring distribution protons n_{pr}/n_{e0} inside the simulation domain.

V_R comparable to the Alfven speed V_A provides free energy to excite magnetosonic waves. The excitation of magnetosonic waves by a proton ring distribution in a uniform magnetized plasma has been thoroughly studied using 1-D particle-in-cell (PIC) simulations (Chen et al., 2016; Liu et al., 2011; Sun, Gao, Lu, et al., 2016). The PIC simulations (e.g., Chen et al., 2016) show that the wave spectrum of the excited magnetosonic waves may change from discrete bands to continuous bands with the decrease of the wave normal angle or when the growth rate is sufficiently large. Recent 1-D PIC simulation (Sun et al., 2017) demonstrates that cool protons and cool electrons can be significantly heated by the magnetosonic waves. However, all these PIC simulations were performed in a homogeneous plasma, and the self-consistent excitation and propagation characteristics of equatorial magnetosonic waves remains unknown in an inhomogeneous dipole magnetic field, which is critical in understanding their roles in scattering relativistic electrons. In this letter, we first describe a two-dimensional (2-D) general curvilinear PIC simulation in the dipole field in section 2 and then present simulation results in section 3, followed by conclusions and discussion in section 4.

2. Two-Dimensional PIC Simulation Model

A 2-D general curvilinear PIC simulation model is used to study the excitation of magnetosonic waves in a dipole field. The general curvilinear PIC simulation model has been used to successfully reproduce chorus emissions in a 2-D mirror field (Ke et al., 2017), where only electron particles are considered. This model has been extended to use a dipole field and to include multiple species. In the modified PIC simulation, both ions and electrons are treated as particles, and the electromagnetic fields are defined on the 2-D grids. The 2-D simulations are run using a grid based on a modified dipole coordinate system in which the first coordinate r in the meridional plane denotes L shell in the dipole field, the second coordinate q varies along a dipole magnetic field, and the third coordinate s is pointed azimuthally. The coordinate q is determined by the following equation:

$$12q^3 + q = \frac{L_0^2 \sin\lambda}{R}, \tag{1}$$

where R is the distance from the Earth in units of Earth radii, λ is the magnetic latitude, and L_0 is the center L shell of interest; $q = 0$ corresponds to the magnetic equator. In the simulation, both electromagnetic fields and particle velocities retain the third component along the azimuthal direction s. The computational domain chosen is illustrated by the black area of Figure 1a in the Cartesian (x, z) coordinates in the meridian plane. The simulation domain consists of a 1,024 by 1,024 grid of evenly distributed bins in the ranges $[0.8, 1.2]$ and $[-0.15, 0.15]$ directions in the r and q directions, respectively. The value of $q = 0.15$ for the center L_0 corresponds to $\lambda \approx 10°$. The r range is centered at $L_0 = 1$ in our simulation, whose spatial inhomogeneity is 4–6 times larger than that of the realistic inner magnetosphere. In this way, we can save computational time by scaling down the simulation domain (using the dipole field line configuration centered at $L_0 = 1$ but with magnetic field strength there reduced to that for $L = 5$ at the equator of the realistic dipole) and reduce artificial electron heating, which requires that the grid size should be comparable to, if not smaller than, the

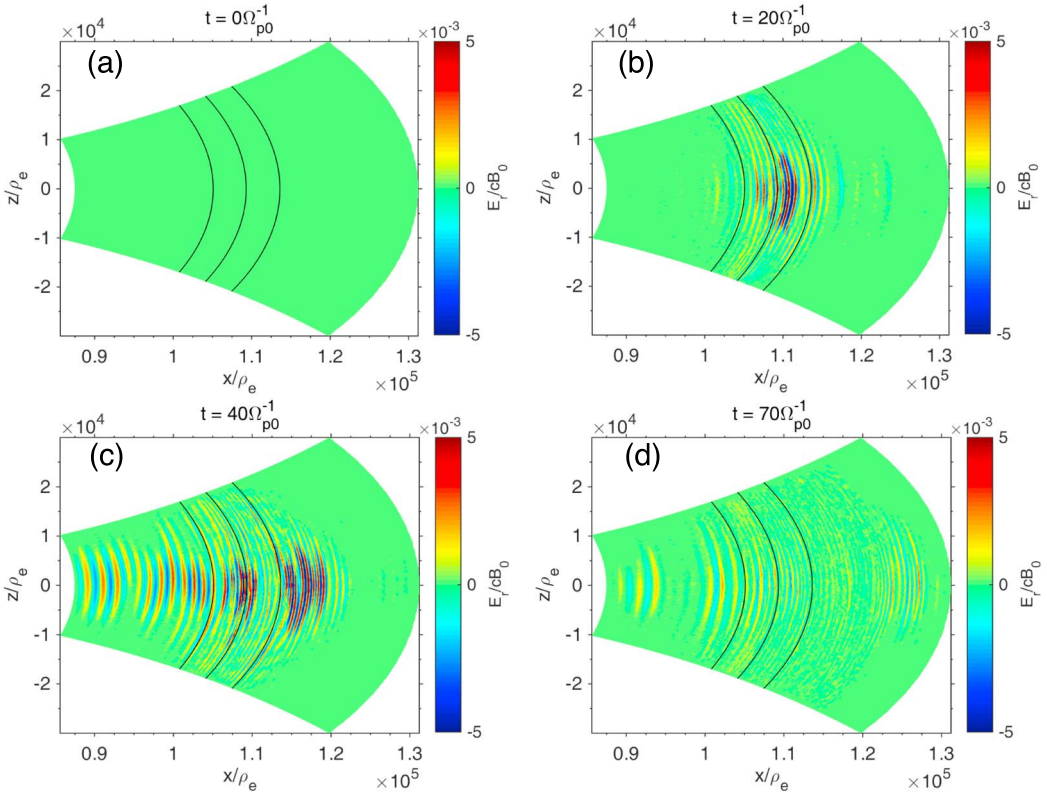

Figure 2. The spatial distribution of the radial component of fluctuating electric fields, E_r/cB_0 at (a) $\Omega_{p0}t = 0$, (b) $\Omega_{p0}t = 20$, (c) $\Omega_{p0}t = 40$, and (d) $\Omega_{p0}t = 70$. The three solid lines in each panel are selected field lines for reference purpose.

electron Debye length. The purpose of the current study is to investigate the excitation and propagation of magnetosonic waves in an inhomogeneous dipole field rather than a direct comparison against actual observation in the magnetosphere.

For initial condition, the plasma consists of three components: a Maxwellian distribution of cool electrons and protons, respectively, and a tenuous (and gyrotropic) ring distribution of protons. Hereafter, subscripts *e*, *pc*, and *pr* represent cool electrons, cool protons, and ring distribution protons, respectively. The cool electrons are initialized to have uniformly distributed number density n_{e0} and thermal speed w_e. The ring distribution protons, as the free energy for magnetosonic waves, are distributed locally with number density $n_{\rm pr}$ peaking near the equator of the domain center L_0 and described below. The cool protons are assumed to have uniformly distributed temperature equal to cool electron temperature and number density $n_{\rm pc} = n_e - n_{\rm pr}$ for the sake of charge neutrality.

In our simulations, the magnetic field and number densities are normalized by the dipole magnetic field B_0 and electron density n_{e0} at the equatorial location of the center field line, that is, $(r, q) = (L_0, 0)$. The time and space are normalized to the inverse of electron gyrofrequency Ω_{e0}^{-1} and the electron gyroradius $\rho_{e0} = w_e/\Omega_{e0}$ (where w_e is the thermal speed of the cool electrons) at that location, respectively. The time step Δt is set as $\Omega_{e0}\Delta t = 0.05$. For reducing computational cost, the mass ratio of proton to electron is reduced such that $m_p/m_e = 100$, and the speed of light is also reduced to be $c = 20V_{A0}$, where $V_{A0} = B_0/\sqrt{\mu_0 n_{e0} m_p}$ is the Alfven speed at the central location of the simulation region. For the chosen values of m_p/m_e and c/V_{A0}, the proton gyrofrequency $\Omega_{p0} = 0.01\Omega_{e0}$ and electron plasma frequency $\omega_{pe} = 200\Omega_{p0}$. The effects of using artificially lower values of c and m_p/m_e, which have been investigated thoroughly in Sun, Gao, Chen, et al. (2016) and Sun, Gao, Lu, et al. (2016), reduce the lower hybrid resonance frequency ($\omega_{\rm LHR} = \Omega_p(m_e/m_p + (V_A/c)^2)^{-1/2}$) and thus tend to scale down the number of ion gyrofrequency harmonics excited as $\omega_{\rm LHR}$ is scaled down.

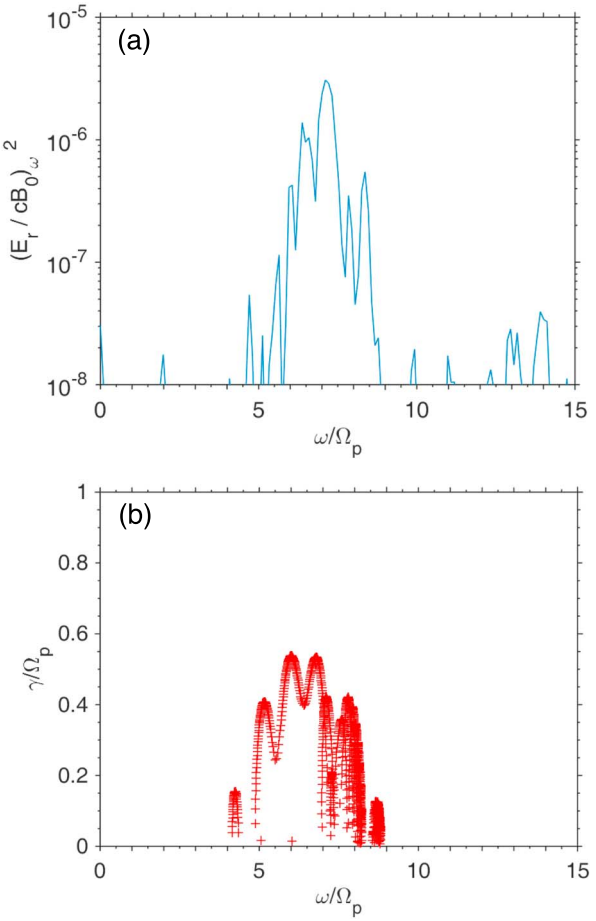

Figure 3. (a) The power spectrum density of the simulated radial component of fluctuating electric fields E_r/cB_0 at the central position $(r, q) = (L_0, 0)$ over the time interval from $\Omega_{p0}t = 0$ to 60. (b) The normalized linear growth rate γ/Ω_{p0} versus the normalized wave frequency ω/Ω_{p0}, obtained from linear theory using the same parameters as the simulation.

The localized distribution of ring proton velocities at the equator adopts the following form:

$$f_{pr}(v_{pr||}, v_{pr,\perp}) = \frac{n_{pr,eq}(r)}{(2\pi)^{3/2} w_{pr}^3} \exp\left(-\frac{(v_{pr\perp} - V_R)^2}{2w_{pr}^2}\right) \exp\left(-\frac{v_{pr||}^2}{2w_{pr}^2}\right), \quad (2)$$

where $v_{pr||}$ and $v_{pr\perp}$ are velocities parallel and perpendicular to the dipole magnetic field, w_{pr} is the thermal speed of the ring distribution, V_R is the proton ring velocity, and $n_{pr,eq}$ is the number density of the ring distribution proton at the equator. The equatorial distribution, $n_{pr,eq}$(r), adopts the form of

$$n_{pr,eq} = n_{pr0} \frac{-\tanh(\frac{r-L_0-l}{\delta}) + \tanh(\frac{r-L_0+l}{\delta})}{-\tanh(\frac{-l}{\delta}) + \tanh(\frac{+l}{\delta})}, \quad (3)$$

where $l = \Delta L/30$ and $\delta = \Delta L/80$. ΔL denotes the radial width of proton ring density distribution. The ring proton number density at the central position $(r, q) = (L_0, 0)$ $n_{pr0} = 0.05 n_{e0}$. The proton ring velocity is initialized as $V_R = V_A$, and the thermal speed of ring distribution protons is $w_{pr} = 0.1 V_A$. The distribution function of the ring protons off the equatorial region can be obtained based on the Liouville's theorem, that is, phase space density is conserved along the particle bounce motion (constant energy and constant magnetic moment). Figure 1b shows the normalized number density of ring distribution protons n_{pr}/n_{e0} in the computation domain at the initial time. The ring distribution protons are concentrated around $(r, q) = (L_0, 0)$, where $L_0 = 1$ for the computational limitation mentioned above. The thermal speed of cool electrons is $w_e = 0.08 V_A$, and the initial electron plasma beta at the position $(r, q) = (L_0, 0)$ is $\beta_e = 1.32 \times 10^{-4}$. When translated to the physical setup, the central field line corresponds to $L = 5$ (except the field line configuration) and $B_0 = 248$ nT, $n_{e0} = 10\ \mathrm{cm}^{-3}$, $V_{A0} = 1.7 \times 10^6$ m/s, cold electron and proton temperature is 1 eV, $\rho_{e0} = 58$ m, $\Omega_{e0} = 2.4 \times 10^3$ rad/s, and $\Omega_{p0} = 24$ rad/s.

For the simulation setup above, the grid size in the Cartesian (x, z) plane $\Delta x \approx \Delta z = 2.2 - 5.2\rho_e$. Every cell has on average 100 macroparticles, whose initial positions are randomly assigned within the cell, for each of the three species. The absorbing boundary conditions for electromagnetic fields are used in both the r and q directions, and reflecting boundary conditions are assumed for particles.

3. Simulation Results

With the general curvilinear 2-D PIC simulation model and the simulation setup described above, we present the excitation of magnetosonic waves by ring distribution protons in the dipole magnetic field. For the purpose of illustration, t is normalized by Ω_{p0}^{-1}, electric field **E** is normalized by cB_0, and the wave frequency ω is normalized by Ω_{p0}.

Figure 2 shows the spatial distribution of the radial electric field component E_r/cB_0 at $\Omega_{p0}t = 0$, 20, 40, and 70. This electric field component is dominant over the other two components. Waves are excited inside the source region of ring distribution protons near $\Omega_{p0}t = 20$ (Figure 2b), with wave intensity concentrated near the equator and nearly constant wave phase fronts along the field lines, implying that exact perpendicular direction of wave number is dominant. Asymmetry in wave power about the equator is also seen, due to random velocity initialization of the prescribed proton ring distribution. It is interesting to note that the wave field does not present sinusoidal variation along the field line. Instead, the wave field simply decays away from the equator. The lack of the wave cycle along the field line direction has been shown to cause transit time scattering (Bortnik & Thorne, 2010) as electrons pass through the edge of equatorially confined wave field during their bounce motions. As time increases, the fluctuating electric fields are able to propagate both inward and outward radially (Figure 2c), allowing the presence of wave intensity beyond the localized proton ring source region. The amplitude of the fluctuating electric fields reaches the maximum at about

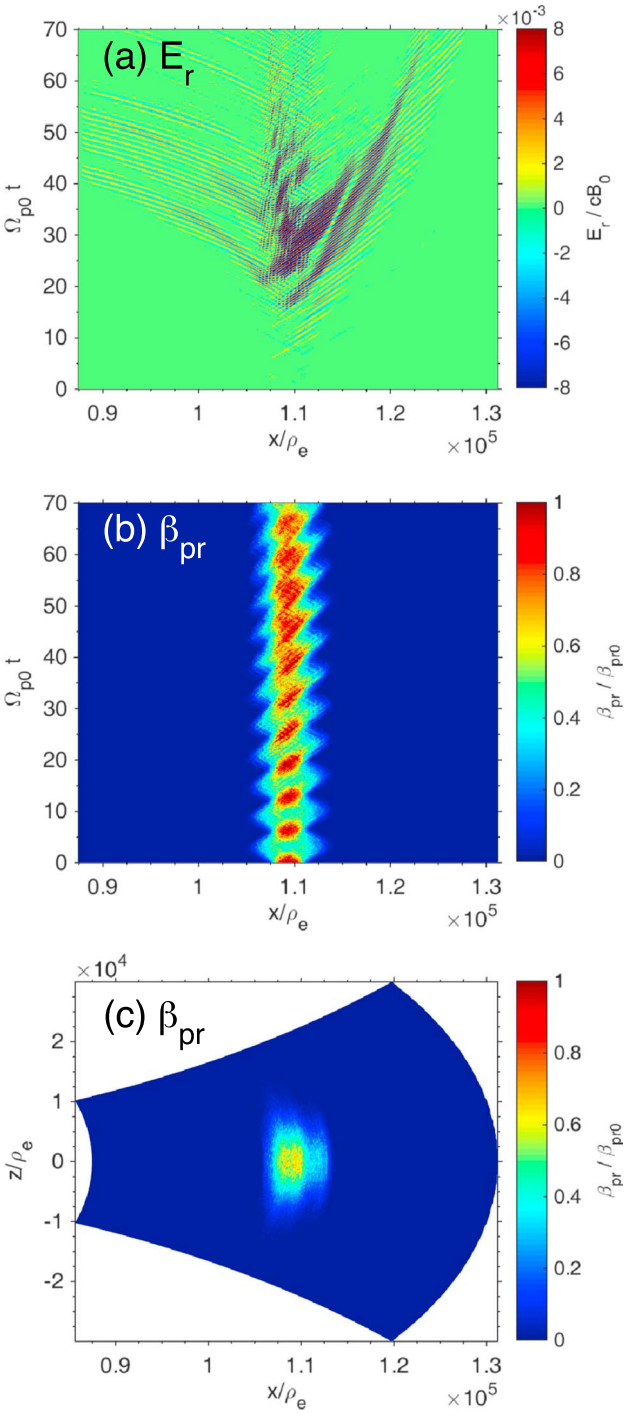

Figure 4. The temporal evolution of (a) the radial component of fluctuating electric fields E_r/cB_0 and (b) the plasma beta of ring distribution protons at the equator as a function of radial distance. (c) The 2-D spatial distribution of the proton ring plasma beta at the end of the simulation $t = 70\Omega_{p0}^{-1}$.

$\Omega_{p0}t = 40$, and then begins to decrease due to the relaxation of the unstable proton ring and the damping by the background plasma (shown later).

To further confirm that the excited fluctuations are magnetosonic waves, we also diagnose the fluctuating magnetic fields. The fluctuating magnetic field in the q direction (the field line direction) is much larger than in the s direction (azimuthal direction) and the r direction (radial direction). In other words, the waves possess compressional magnetic field and a nearly linear polarization, which is consistent with the magnetosonic waves excited by ring distribution protons in a homogeneous plasma (Chen et al., 2016; Liu et al., 2011, Sun, Gao, Lu, et al., 2016). To verify this, we compare the simulation results against the linear theory. Figure 3a shows the wave spectrum of the radial component of fluctuating electric fields $(E_r/cB_0)_w^2$ at the central position $(r, q) = (L_0, 0)$, which is calculated by Fourier transforming of time series of fluctuating electric fields E_r/cB_0 over the time interval from $\Omega_{p0}t = 0$ to 60. Figure 3b shows the linear growth rate γ/Ω_{p0} of the perpendicular propagating magnetosonic waves versus the wave frequency ω/Ω_{p0}, calculated using the initial plasma parameters at the same location and using the same choice of the m_p/m_e ratio and the c value. The frequency range of intense wave power spectrum density $(E_r/cB_0)_w^2$ in our simulations, 4–9 Ω_{p0}, agrees well with that of positive growth rate predicted by the linear theory. Both also consistently present the same frequency peak at $\omega/\Omega_{p0} = 7$. The magnitude of linear growth rate ($\sim 0.5\Omega_{p0}$) is also comparable to the growth rate ($\sim 0.3\Omega_{p0}$) estimated from examining the temporal profile of the radial electric field component $(E_r/cB_0)^2$ during the wave growth phase $0-30\Omega_{p0}^{-1}$ (Figure 4a). One discrepancy is the presence of a weak second harmonic in the simulation, which is not unstable according to the linear theory. The formation of the relatively weak second harmonics may be caused by the nonlinear wave-wave coupling (Chen et al., 2016; Gao et al., 2018). Based on the diagnosis of wave properties and the comparison with the linear theory, it is safe to conclude that the excited fluctuating electromagnetic fields in our simulations are indeed magnetosonic wave mode generated by the proton ring distribution. We also note that wave spectra do not necessarily peak at the harmonics of local proton gyrofrequency, for example, at 5 and 8 Ω_{p0}, due to wave propagation effect, which is consistent with the finding of Shklyar and Balikhin (2017).

Since the waves are confined near the equator, we examine the evolution of particles and waves at the equator. Figure 4a shows the evolution of the radial component of fluctuating electric fields E_r/cB_0 at the equator ($q = 0$). Figure 4b shows corresponding temporal evolution of the plasma beta of ring distribution protons $\beta_{pr} = 2\mu_0 n_{pr} T_{pr}/B_0^2$ at the equator, which represents the energy density of ring distribution protons. The temperature T_{pr} of ring distribution protons in every grid cell is calculated by

$$T_{pr} = m_p \left\langle \left(\mathbf{v}_{pr} - \left\langle \mathbf{v}_{pr} \right\rangle\right) \cdot \left(\mathbf{v}_{pr} - \left\langle \mathbf{v}_{pr} \right\rangle\right) \right\rangle,$$

where the angle brackets denote an average over particles of a given species inside a cell. One can see that as the magnetosonic waves are excited, the plasma beta of the ring distribution protons tends to decrease (Figure 4a) and become extended in the radial direction at the end of the simulation $t = 70\Omega_{p0}^{-1}$ (Figure 4c). The apparent periodic oscillation of the plasma beta at the proton cyclotron period arises due to the inhomogeneity nature of the radially localized distribution of the proton ring. The excited waves are able to propagate away from the source region both radially inward and outward (Figure 4a). One can see that the waves inside the excitation region

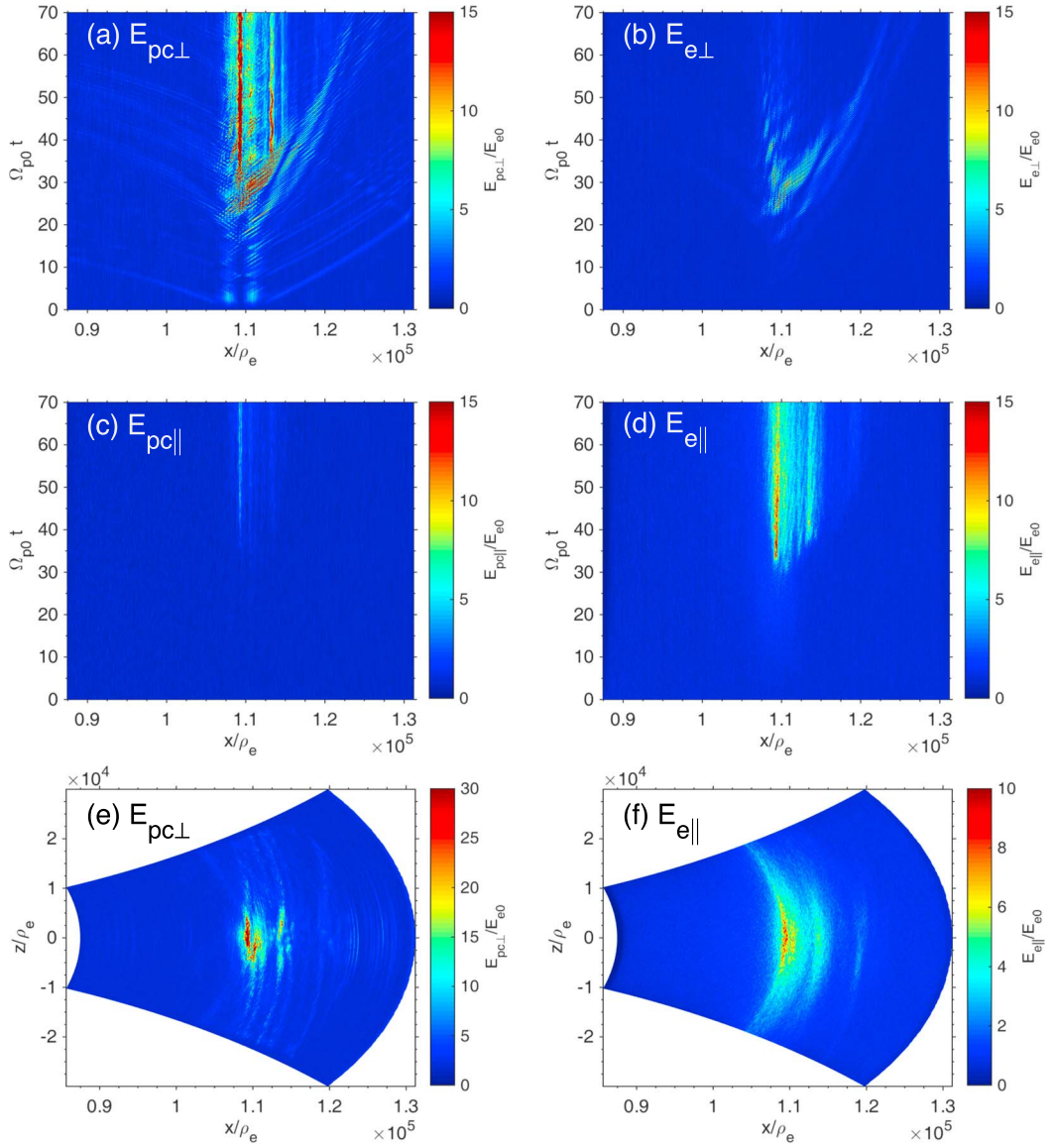

Figure 5. The temporal evolution of (a) the perpendicular kinetic energy of cool protons, (c) the parallel kinetic energy of cool protons, (b) the perpendicular kinetic energy of cool electrons, and (d) the parallel kinetic energy of cool electrons at the equator. Also shown are the 2-D spatial distribution at the end of the simulation $t = 70\Omega_{p0}^{-1}$ of the perpendicular kinetic energy of cool protons (e) and the parallel kinetic energy of cool electrons (f).

propagate bidirectionally, while once away from the source region, the waves propagate unidirectionally, either inward or outward depending on the sides of the source region. Also, the inward propagation speed is larger than that toward the outward propagation speed (because of the greater magnetic field strength), leading to the asymmetric distribution of the magnetosonic wave intensity between two sides of the source region. Typically, waves propagate over a radial distance of $\sim 0.1 \times 10^5 \rho_e$ on a timescale of $10\Omega_{p0}^{-1}$ (Figure 4a), equivalent to group speed at 0.8 V_{A0}. Such estimate is also consistent with propagation speed of magnetosonic waves.

Finally, we examine temporal and spatial evolution of kinetic energy distribution (Figure 5) for different species at the equator ($q = 0$), the perpendicular kinetic energy of cool protons (Figure 5a), the parallel kinetic energy of cool protons (Figure 5c), the perpendicular kinetic energy of cool electrons (Figure 5b), and the parallel kinetic energy of cool electrons (Figure 5d), all of which are normalized by the initial electron energy $E_{e0} =$

$m_e w_e^2$. The perpendicular and parallel temperature of species j (cool electrons or cool protons) is calculated as

$$T_{j\perp} = m_j \left\langle (\mathbf{v}_{j\perp} - \langle \mathbf{v}_{j\perp} \rangle) \cdot (\mathbf{v}_{j\perp} - \langle \mathbf{v}_{j\perp} \rangle) \right\rangle$$

and

$$T_{j\parallel} = m_j \left\langle (\mathbf{v}_{j\parallel} - \langle \mathbf{v}_{j\parallel} \rangle) \cdot (\mathbf{v}_{j\parallel} - \langle \mathbf{v}_{j\parallel} \rangle) \right\rangle,$$

where the angle brackets denote an average over particles of species j inside a cell. Both the cool protons and electrons can be energized but with different preferential directions. For cool protons, the energization only occurs in the perpendicular direction with little energization in the parallel direction. The perpendicular heating of cool protons is due to harmonic cyclotron resonance. On the other hand, these cool electrons can be efficiently heated in the parallel direction, possibly due to the phase mixing of dispersive magnetosonic waves (Sun et al., 2017), and the apparent perpendicular energization is associated with electron perpendicular $\mathbf{E}\times\mathbf{B}$ drift due to wave electric field. As the waves are strongest near $\Omega_{p0}t = 40$, electron perpendicular kinetic energy reaches the maximum, while as the waves decay later, the perpendicular energy vanishes because of weakening $\mathbf{E} \times \mathbf{B}$ drift. The energization characteristics found in our 2-D simulation of the cool protons and electrons are consistent with previous 1-D simulation in a homogeneous plasma (Sun et al., 2017), which offers detailed diagnosis and detailed explanation. One noteworthy point in our 2-D simulation is that cool electron and proton energization is more efficient near the source region than outside the source region (Figures 5e and 5f), because of the greater wave intensity inside. This may serve as additional signatures useful for determining whether the waves are in the source region or not in the real observation such as Van Allen Probes. Although plasma beta oscillates at the frequency of $1\Omega_p$ due to the inhomogeneity of proton ring radial distribution as mentioned above, we did not observe significant power spectral density near $1\Omega_p$ (Figure 3a), or electrostatic Langmuir waves in the simulation, which could otherwise be another potential source of the cool particle heating. In addition, good agreement is demonstrated between the linear theory and the simulation for both aspects of wave spectra (Figure 3) and wave growth rate (as discussed above), which also suggests a limited role of plasma beta oscillation in the simulation of magnetosonic waves of interest.

4. Conclusions and Discussion

In this letter, we present for the first time a 2-D general curvilinear PIC simulation of the excitation of magnetosonic waves in a dipole magnetic field and in the plasma consisting of three components: cool electrons and protons and tenuous ring distribution protons. Our principal conclusions are summarized as follows:

- The magnetosonic waves are excited inside the source region of the proton ring distribution. They are confined near the equator, with wave phase front aligned with the field line and wave intensity decaying away from the equator.
- The waves propagate perpendicularly, with bidirectional (inward and outward) propagation inside the source region and with a single propagation direction outside the source region. The simulated wave fields show asymmetry between the inner and outer sides of the source region because of different magnetic field strength and thus different propagation speeds.
- Excited magnetosonic waves lead to perpendicular heating of the cool protons and parallel heating of cool electrons. The heating due to magnetosonic waves is most efficient inside the source region.

The computational cost limits us to consider the PIC simulation with less realistic parameters, for instance, the choice of $L_0 = 1$, the smaller ratio m_p/m_e, and the smaller speed of light c than the actual value. Several improvements, such as using more realistic parameters and minimizing oscillation of localized plasma beta, are left as future work. Despite these, we aim at understanding general characteristics of magnetosonic waves excitation in the inhomogeneous plasma. We also present careful analysis to make sure the conclusions we obtain above are sound in physics. The current simulation enables us to learn much more from the 2-D simulation in the inhomogeneous plasma, which self-consistently deals with wave excitation, wave propagation, and plasma heating, than from the 1-D simulation in a homogeneous plasma. It is interesting to note that plasma density variation plays a significant role in affecting both radial propagation (e.g., Liu et al., 2018) and characteristics of wave growth and damping (e.g., Chen, Thorne, Jordanova, Wang, et al., 2010; Yuan et al., 2017). Self-consistent simulation of the plasma density variation effects will be performed in future work.

Acknowledgments
This research was supported by the NSFC grants 41604128, 41631071, 41331067, 41421063, and 41574139 and Key Research Program of Frontier Sciences, CAS (QYZDJ-SSW-DQC010). L. C. acknowledges the support of NSF-GEM grant AGS-1705079, grant 32955099, and AFOSR grant FA9550-16-1-0344. The simulation data are available via the link https://pan.baidu.com/s/1hjV5hCxKpOxbcOr-VtpZLg. No observational data are used.

References

Balikhin, M. A., Shprits, Y. Y., Walker, S. N., Chen, L., Cornilleau-Wehrlin, N., Dandouras, I., et al. (2015). Observations of discrete harmonics emerging from equatorial noise. *Nature Communications*, *6*, 7703. https://doi.org/10.1038/ncomms8703

Boardsen, S. A., Gallagher, D. L., Gurnett, D. A., Peterson, W. K., & Green, J. L. (1992). Funnel-shaped, low-frequency equatorial waves. *Journal of Geophysical Research*, *97*(14), 14,967–14,976. https://doi.org/10.1029/92JA00827

Boardsen, S. A., Hospodarsky, G. B., Kletzing, C. A., Pfaff, R. F., Kurth, W. S., Wygant, J. R., & MacDonald, E. A. (2014). Van Allen Probe observations of periodic rising frequencies of the fast magnetosonic mode. *Geophysical Research Letters*, *41*, 8161–8168. https://doi.org/10.1002/2014GL062020

Bortnik, J., & Thorne, R. M. (2010). Transit time scattering of energetic electrons due to equatorially confined magnetosonic waves. *Journal of Geophysical Research*, *115*, A07213. https://doi.org/10.1029/2010JA015283

Bortnik, J., Thorne, R. M., Ni, B., & Li, J. (2015). Analytical approximation of transit time scattering due to magnetosonic waves. *Geophysical Research Letters*, *42*, 1318–1325. https://doi.org/10.1002/2014GL062710

Chen, L. (2015). Wave normal angle and frequency characteristics of magnetosonic wave linear instability. *Geophysical Research Letters*, *42*, 4709–4715. https://doi.org/10.1002/2015GL064237

Chen, L., Maldonado, A., Bortnik, J., Thorne, R. M., Li, J., Dai, L., & Zhan, X. (2015). Nonlinear bounce resonances between magnetosonic waves and equatorially mirroring electrons. *Journal of Geophysical Research: Space Physics*, *120*, 6514–6527. https://doi.org/10.1029/2015JA021174

Chen, L., Thorne, R. M., Bortnik, J., & Zhang, X.-J. (2016). Nonresonant interactions of electromagnetic ion cyclotron waves with relativistic electrons. *Journal of Geophysical Research: Space Physics*, *121*, 9913–9925. https://doi.org/10.1002/2016JA022813

Chen, L., Thorne, R. M., Jordanova, V. K., & Horne, R. B. (2010). Global simulation of magnetosonic wave instability in the storm time magnetosphere. *Journal of Geophysical Research*, *115*, A11222. https://doi.org/10.1029/2010JA015707

Chen, L., Thorne, R. M., Jordanova, V. K., Wang, C., Gkioulidou, M., Lyons, L., & Horne, R. B. (2010). Global simulation of EMIC wave excitation during the 21 April 2001 storm from coupled RCM-RAM-HOTRAY modeling. *Journal of Geophysical Research*, *115*, A07209. https://doi.org/10.1029/2009JA015075

Curtis, S. A., & Wu, C. S. (1979). Gyroharmonic emissions induced by energetic ions in the equatorial plasmasphere. *Journal of Geophysical Research*, *84*, 2597–2607. https://doi.org/10.1029/JA084iA06p02597

Gao, X., Sun, J., Lu, Q., Chen, L., & Wang, S. (2018). Generation of lower harmonic magnetosonic waves through nonlinear wave-wave interactions. *Geophysical Research Letters*, *45*. https://doi.org/10.1029/2018GL079090

Gul'elmi, A., Klaine, B., & Potapov, A. (1975). Excitation of magnetosonic waves with discrete spectrum in the equatorial vicinity of the plasmapause. *Planetary and Space Science*, *23*(2), 279–286. https://doi.org/10.1016/0032-0633(75)90133-6

Gurnett, D. A. (1976). Plasma wave interactions with energetic ions near the magnetic equator. *Journal of Geophysical Research*, *81*, 2765–2770. https://doi.org/10.1029/JA081i016p02765

Horne, R. B., Thorne, R. M., Glauert, S. A., Meredith, N. P., Pokhotelov, D., & Santolík, O. (2007). Electron acceleration in the Van Allen radiation belts by fast magnetosonic waves. *Geophysical Research Letters*, *34*, L17107. https://doi.org/10.1029/2007GL030267

Ke, Y., Gao, X., Lu, Q., Wang, X., & Wang, S. (2017). Generation of rising-tone chorus in a two-dimensional mirror field by using the general curvilinear pic code. *Journal of Geophysical Research: Space Physics*, *122*, 8154–8165. https://doi.org/10.1002/2017JA024178

Li, J., Ni, B., Ma, Q., Xie, L., Pu, Z., Fu, S., et al. (2016). Formation of energetic electron butterfly distributions by magnetosonic waves via Landau resonance. *Geophysical Research Letters*, *43*, 3009–3016. https://doi.org/10.1002/2016GL067853

Li, J., Ni, B., Xie, L., Pu, Z., Bortnik, J., Thorne, R. M., et al. (2014). Interactions between magnetosonic waves and radiation belt electrons: Comparisons of quasi-linear calculations with test particle simulations. *Geophysical Research Letters*, *41*, 4828–4834. https://doi.org/10.1002/2014GL060461

Li, X., Tao, X., Lu, Q., & Dai, L. (2015). Bounce resonance diffusion coefficients for spatially confined waves. *Geophysical Research Letters*, *42*, 9591–9599. https://doi.org/10.1002/2015GL066324

Liu, X., Chen, L., Yang, L., Xia, Z., & Malaspina, D. M. (2018). One-dimensional full wave simulation of equatorial magnetosonic wave propagation in an inhomogeneous magnetosphere. *Journal of Geophysical Research: Space Physics*, *123*, 587–599. https://doi.org/10.1002/2017JA024336

Liu, K., Gary, S. P., & Winske, D. (2011). Excitation of magnetosonic waves in the terrestrial magnetosphere: Particle-in-cell simulations. *Journal of Geophysical Research*, *116*, A07212. https://doi.org/10.1029/2010JA016372

Ma, Q., Li, W., Chen, L., Thorne, R. M., & Angelopoulos, V. (2014). Magnetosonic wave excitation by ion ring distributions in the Earth's inner magnetosphere. *Journal of Geophysical Research: Space Physics*, *119*, 844–852. https://doi.org/10.1002/2013JA019591

McClements, K. G., Dendy, R. O., & Lashmore-Davies, C. N. (1994). A model for the generation of obliquely propagating ULF waves near the magnetic equator. *Journal of Geophysical Research*, *99*(A12), 23,685–23,693. https://doi.org/10.1029/94JA01979

Meredith, N. P., Horne, R. B., & Anderson, R. R. (2008). Survey of magnetosonic waves and proton ring distributions in the Earth's inner magnetosphere. *Journal of Geophysical Research*, *113*, A06213. https://doi.org/10.1029/2007JA012975

Min, K., & Liu, K. (2016). Understanding the growth rate patterns of ion Bernstein instabilities driven by ring-like proton velocity distributions. *Journal of Geophysical Research: Space Physics*, *121*, 3036–3049. https://doi.org/10.1002/2016JA022524

Min, K., Liu, K., Wang, X., Chen, L., & Denton, R. E. (2018). Fast magnetosonic waves observed by Van Allen Probes: Testing local wave excitation mechanism. *Journal of Geophysical Research: Space Physics*, *123*, 2169–9402. https://doi.org/10.1002/2017JA024867

Perraut, S., Roux, A., Robert, P., Gendrin, R., Sauvaud, J., Bosqued, J., et al. (1982). A systematic study of ULF waves above F/H plus/ from GEOS 1 and 2 measurements and their relationships with proton ring distributions. *Journal of Geophysical Research*, *87*, 6219–6236. https://doi.org/10.1029/JA087iA08p06219

Russell, C. T., Holzer, R. E., & Smith, E. J. (1970). OGO 3 observations of ELF noise in the magnetosphere. 2. The nature of the equatorial noise.*Journal of Geophysical Research*, *75*, 755–768. https://doi.org/10.1029/JA075i004p00755

Santolík, O., Pickett, J. S., Gurnett, D. A., Maksimovic, M., & Cornilleau-Wehrlin, N. (2002). Spatiotemporal variability and propagation of equatorial noise observed by Cluster. *Journal of Geophysical Research*, *107*, 1495. https://doi.org/10.1029/2001JA009159

Shklyar, D. R., & Balikhin, M. A. (2017). Whistler mode waves below lower hybrid resonance frequency: Generation and spectral features. *Journal of Geophysical Research: Space Physics*, *122*, 10,072–10,083. https://doi.org/10.1002/2017JA024416

Sun, J., Gao, X., Chen, L., Lu, Q., Tao, X., & Wang, S. (2016). A parametric study for the generation of ion Bernstein modes from a discrete spectrum to a continuous one in the inner magnetosphere. I. Linear theory. *Physics of Plasmas*, *23*(2), 022901. https://doi.org/10.1063/1.4941283

Sun, J., Gao, X., Lu, Q., Chen, L., Liu, X., Wang, X., et al. (2017). Spectral properties and associated plasma energization by magnetosonic waves in the Earth's magnetosphere: Particle-in-cell simulations. *Journal of Geophysical Research: Space Physics*, *122*, 5377–5390. https://doi.org/10.1002/2017JA024027

Sun, J., Gao, X., Lu, Q., Chen, L., Tao, X., & Wang, S. (2016). A parametric study for the generation of ion Bernstein modes from a discrete spectrum to a continuous one in the inner magnetosphere. II. Particle-in-cell simulations. *Physics of Plasmas*, *23*(2), 022902. https://doi.org/10.1063/1.4941284

Tao, X., & Li, X. (2016). Theoretical bounce resonance diffusion coefficient for waves generated near the equatorial plane. *Geophysical Research Letters*, *43*, 7389–7397. https://doi.org/10.1002/2016GL070139

Tsurutani, B. T., Falkowski, B. J., Pickett, J. S., Verkhoglyadova, O. P., Santolik, O., & Lakhina, G. S. (2014). Extremely intense ELF magnetosonic waves: A survey of polar observations. *Journal of Geophysical Research: Space Physics*, *119*, 964–977. https://doi.org/10.1002/2013JA019284

Yuan, Z., Yu, X., Huang, S., Wang, D., & Funsten, H. O. (2017). In situ observations of magnetosonic waves modulated by background plasma density. *Geophysical Research Letters*, *44*, 7628–7633. https://doi.org/10.1002/2017GL074681